frontiers in Materials

ORIGINAL RESEARCH
published: 04 July 2019
doi: 10.3389/fmats.2019.00160

Post-processing Methods to Improve Strength of Particle-Bed 3D Printed Geopolymer for Digital Construction Applications

Behzad Nematollahi, Ming Xia* and Jay Sanjayan*

Centre for Smart Infrastructure and Digital Construction, Faculty of Science, Engineering and Technology, Swinburne University of Technology, Hawthorn, VIC, Australia

The strength of powder-based 3D printed geopolymer samples immediately after the de-powdering process ("green" strength) is inherently very low. Therefore, different post-processing techniques have been explored in the previous study of the authors to enhance the "green" strength of the printed geopolymer. The highest strength of around 30 MPa was achieved for the printed slag-based geopolymer sample cured in an alkaline solution for 7 days at 60°C. Although this strength is sufficient for a wide range of construction applications, the necessity for the heat curing procedure, which requires a significant amount of energy, can compromise the sustainability credentials of the developed powder-based 3D printed geopolymer and limit its commercial viability and large-scale applications in the construction industry. To tackle this issue, this study aims to develop a new post-processing method which eliminates the necessity for the heat curing. The influences of type of curing medium, duration and temperature of curing, and testing direction on the compressive strength of the printed geopolymer were investigated. The "green" printed geopolymer samples were immersed in four different curing mediums, including two sodium (Na)-based, and two potassium (K)-based activators with different alkali modulus (SiO_2/M_2O where M = Na or K), and cured at two different curing temperatures (ambient temperature (23°C) vs. 60°C) for 7 and 28 days. The compressive strength of the "post-processed" printed geopolymer specimens was measured in two different testing directions, namely the binder jetting direction and layer stacking direction. The results showed that the 28-day compressive strength of the ambient temperature cured printed geopolymer sample was comparable to the 7-day compressive strength of the corresponding heat cured sample. Therefore, the feasibility of enhancing the strength of printed geopolymer by curing in an alkaline solution at ambient temperature was established. This developed post-processing method based on the ambient temperature curing is more viable and less energy-intensive, yet provides comparable strength, as compared to the previously developed post-processing method based on the heat curing. The results also showed that the strength of the printed geopolymer samples cured in the K-based activators was lower than that of the specimens cured in the Na-based activators.

Keywords: geopolymer, 3D concrete printing, digital construction, post-processing, powder-based 3D printing

OPEN ACCESS

Edited by:
John L. Provis, University of Sheffield, United Kingdom

Reviewed by:
Jadambaa Temuujin, Mongolian Academy of Sciences (MAS), Mongolia
Alastair T. M. Marsh, University of Leeds, United Kingdom

****Correspondence:***
Behzad Nematollahi
bnematollahi@swin.edu.au
Ming Xia
mxia@swin.edu.au

Specialty section:
This article was submitted to Structural Materials, a section of the journal Frontiers in Materials

Received: *05 February 2019*
Accepted: *21 June 2019*
Published: *04 July 2019*

Citation:
Nematollahi B, Xia M and Sanjayan J (2019) Post-processing Methods to Improve Strength of Particle-Bed 3D Printed Geopolymer for Digital Construction Applications. Front. Mater. 6:160. doi: 10.3389/fmats.2019.00160

INTRODUCTION

3D Concrete Printing (3DCP), a digitally layer-by-layer manufacturing process, has recently begun to draw significant attention in the construction industry (Wu et al., 2016; Nematollahi et al., 2017c). As an emerging field of additive manufacturing, 3DCP has the potential to revolutionize the construction industry (Wangler et al., 2016). This technology can bring significant benefits to the current construction industry such as increasing geometrical flexibility, adding multi-functionalities, eliminating the use of formwork, and a considerable reduction in construction cost and time (Wangler et al., 2016). Although this technology is still in its infant stages of realization in the construction industry, numerous studies have been conducted on the related areas for better utilization in the future.

Two common 3DCP techniques are used in the current construction industry, namely extrusion-based 3DCP and powder-based 3DCP (also known as particle-bed 3DCP). The extrusion-based 3DCP is a selective material deposition technique aimed for on-site concrete construction. In this technique, the cementitious material is extruded by a digitally controlled extruder to manufacture the component layer-by-layer [e.g., Contour Crafting (Khoshnevis, 2004), Concrete Printing (Le et al., 2012a,b)]. In this process, the material must be fluid enough during the transferring in the pumping system and must have sufficient viscosity and yield stress to keep the shape after being extruded out. Not only large-scale buildings, such as houses, could be built using this method, but also this could be achieved without any formwork. Formwork is the temporary structure and mold for pouring wet concrete, typically built with timber. The cost of formwork is estimated to be between 35 and 60% of the overall cost of concrete construction (Lloret et al., 2015). Besides, formwork represents a source of waste, as all formwork made of timber is discarded sooner or later, contributing to a generally increasing amount of waste in the world (De Schutter et al., 2018; Sanjayan and Nematollahi, 2019).

In the powder-based 3DCP technique a liquid binder (or "Ink") is selectively deposited onto the powder surface to bind the powder particles (e.g., D-Shape (Cesaretti et al., 2014), Emerging Objects (Rael and San Fratello, 2011) which enables the production of complex structures with subtle details and intricate shapes. This technique which is aimed for off-site construction is highly suitable for the manufacture of small-scale building components such as panels, permanent formworks and interior structures that then can later be assembled on site. One of the important advantages of the powder-based 3DCP technique, as compared to the extrusion-based technique, is that structures with overhang parts can be printed without the necessity of having a support structure, because unbound powder particles can support the printed parts.

In general in 3DCP process, due to the layer-by-layer production process, the deposited layers should gain adequate green strength to support the upper layers without significant deformation or collapsing. In the extrusion-based 3DCP process, the ability of the deposited layer to sustain its own weight and to support the upper layers is linked to its rheology and more particularly to its yield stress (Roussel, 2018) With regards to the powder-based 3DCP process, according to Shanjani and Toyserkani (2008), the maximum compact pressure occurred in the narrowest gap between the roller and the underneath powder layer was < 0.9 Pa. In other words, the green strength of each printed layer should be more than 0.9 Pa to prevent any deformation during the printing process.

Although the powder-based 3DCP technique can offer numerous advantages in the construction industry, there are several challenges which should be overcome before the technique is fully utilized. One of the main challenges is the severely limited range of printing materials that are suitable for construction applications. It is worth noting that some printing materials have been developed and used in commercial powder-based 3D printers for different applications in other industries. For instance, biocompatible materials including hydroxyapatite (Zhou et al., 2014), tricalcium phosphate (Al-Sanabani et al., 2013; Zhou et al., 2014), calcium sulfate hemihydrate (Asadi-Eydivand et al., 2016) have been used for biomedical applications. Ceramic materials such as barium titanate (Gaytan et al., 2015) and silicon carbide (Moon et al., 2001) have been used for manufacture of electrical components. Inconel 718 (Nandwana et al., 2017) and copper powder (Bai and Williams, 2015) have been used for fabricating metal components. Fine silica sand is used for fabrication of sand molds and cores (ExOne, 2015; Voxeljet, 2016). However, these printing materials are not suitable for construction applications. Therefore, it is urgently needed to develop new printing materials which can be used in the commercially available powder-based 3D printers for construction applications.

Conventional Portland cement has been considered as the master construction material for its high strength and stability, as well as its low cost for over 100 years and will probably be produced and used for at least the next 100 years (Biernacki et al., 2017). However, the slow setting time of Portland cement may limit its use for the powder-based 3DCP process. Few studies have reported the use of other types of cementitious materials. For instance, magnesium oxychloride cement (also known as Sorel cement) (Cesaretti et al., 2014) and fiber reinforced cement polymer (Rael and San Fratello, 2011) were used in D-shape and Emerging Objects, respectively. In addition, Gibbons et al. (Gibbons et al., 2010) conducted a preliminary study to investigate the feasibility of using a mixture of polyvinyl alcohol and rapid hardening Portland cement (RHPC) for the powder-based 3DCP process for the manufacture of biomedical implants. The printed specimens exhibited a maximum modulus of rupture of 2.4 MPa after 26-day water immersion at ambient temperature. The low strength of the developed RHPC powder may limit its use for construction applications. Maier et al. (2011) investigated a mixture of flash-setting calcium aluminate cement (CAC) for powder-based 3D printing to fabricate a bone regeneration scaffold. A compressive strength of up to 20 MPa was reported for the printed specimen after 3-day water immersion.

It is well established that the production of ordinary Portland cement (OPC) is highly energy- and emissions-intensive. As a rule of thumb, production of each ton of OPC would emit about one ton of carbon dioxide (Mccaffrey, 2002). The emissions due

to the manufacture of OPC are the fourth largest source of carbon emissions after petroleum, coal, and natural gas and are estimated to account for 5–7% of all anthropogenic emissions (Huntzinger and Eatmon, 2009). Therefore, it is essential to develop alternative OPC-less binders which would be suitable for the powder-based 3DCP process. To tackle this limitation, the authors of this study have been working on developing innovative methodologies for formulating geopolymer-based materials which can be used in the commercially available powder-based 3D printers for construction applications.

Geopolymer can be manufactured by alkaline activation of industrial by-products such as fly ash and slag. (Nematollahi et al., 2015b). The production of fly ash-based geopolymer can emit up to 80% less carbon dioxide (Duxson et al., 2007) and can consume up to 60% less energy than the production of OPC (Li et al., 2004). It should be pointed out that the environmental impact (i.e., carbon emission and embodied energy) of geopolymer is highly dependent on the specific precursor, and moreover, on the activator used. Apart from the potential environmental benefits of geopolymer as compared to OPC, the authors believe that geopolymer is a highly suitable material for the layer-by-layer build-up process in the powder-based 3DCP technique. This is because geopolymer, as compared to OPC, has more flexibly adjustable setting characteristics and is capable of developing higher strengths in a short period of time (Nematollahi et al., 2015a, 2017b). Many characteristics of geopolymer such as its setting time and strength development can be controlled by manipulating the activation and curing techniques, which can eliminate the necessity for using admixtures for development of 3D printable geopolymers. However, Portland cement is manufactured to comply with strict specifications with regards to setting time, strength development, etc. Therefore, different admixtures are required for the development of 3D printable OPC-based mixtures. The use of admixtures may not only increase the cost but can also have possible side effects and incompatibilities (Marchon et al., 2018).

Several geopolymer-based formulations using slag/fly ash have been developed by the authors which are suitable for the powder-based 3DCP applications (Xia and Sanjayan, 2016, 2018; Xia et al., 2018a,b). The 3D printed samples using the developed geopolymer-based powders are presented in **Figure 1**. It should be noted that in this paper, the term geopolymer is used in its broad meaning to represent alkali-activated cements, although it is understood that some can be alkali-activated slag or fly ash, especially those cured with relatively low alkalinity. This is justified since the term "geopolymer" has become a common-usage-term for alkali-activated cements in the literature (Duxson et al., 2006).

The strength of powder-based 3D printed geopolymer specimens immediately after completion of the de-powdering process often referred to as "green" strength, is typically very low due to the inherently high porosity of the powder bed. Therefore, further post-processing methods are required to increase the strength of the 3D printed geopolymer specimens to be adequate for construction applications. In the authors' previous study (Xia and Sanjayan, 2018), different post-processing procedures have been explored to increase the "green" strength of the powder-based 3D printed geopolymers. According to the results, immersing the printed "green" samples in a combination of sodium silicate solution with SiO_2/Na_2O of 3.22 and 8.0 M sodium hydroxide solutions for 7 days at 60°C resulted in the highest compressive strength of 30 MPa, which is sufficient for a wide range of construction applications (Xia and Sanjayan, 2018).

Although the authors' previously developed post-processing procedure based on the heat curing (Xia and Sanjayan, 2018) significantly improved the final mechanical properties of the 3D printed geopolymer samples, the necessity for the heat curing procedure not only limits the commercial viability and large-scale applications of the developed powder-based 3D printed geopolymers in the construction industry, but also can compromise the sustainability credentials of 3D printed geopolymers. Therefore, the first objective of this study is to investigate the feasibility of developing a new post-processing procedure based on the ambient temperature curing, which eliminates the necessity for heat curing. In this regard, the effect of curing temperature (heat curing vs. ambient temperature curing) on the compressive strength of the powder-based 3D printed geopolymers were investigated.

All alkaline solutions (i.e., curing mediums) used for the post-processing procedure developed in the previous study of the authors (Xia and Sanjayan, 2018) were sodium (Na)-based. The effect of potassium (K)-based curing mediums has not yet been investigated. Therefore, the second objective of this study is to investigate the effect of type of curing medium (Na-based vs. K-based) and alkali modulus (SiO_2/M_2O where M = Na or K) of sodium silicate (Na_2SiO_3) and potassium silicate (K_2SiO_3) solutions on the compressive strength of the powder-based 3D printed geopolymers.

MATERIALS AND EXPERIMENTAL PROCEDURES

Raw Materials

Printable Geopolymer Powder

A printable geopolymer powder previously developed by the authors (Xia and Sanjayan, 2016) was used in this study. **Figure 2** shows the particle size distribution of the printable geopolymer powder obtained using CILAS 1190 laser diffraction particle analyzer.

The printable geopolymer powder was a mixture of slag, ground anhydrous sodium metasilicate powder and fine silica sand. The slag supplied from Independent Cement, Australia was used as the aluminosilicate source material. The chemical composition and loss on ignition (LOI) of the slag was determined by X-ray Fluorescence (XRF), on an ignited mass basis (LOI: 0.09 wt %), as CaO (44.64 wt%) SiO_2 (32.76 wt %), Al_2O_3 (12.37 wt %), MgO (5.15 wt %), SO_3 (4.26 wt %), and others (0.73 wt%). **Figure 3** shows the X-ray diffraction pattern and crystalline phases of slag used in this study. The XRD analysis of slag was carried out using a Bruker D8 Advance X-ray diffractometer (Bruker, Germany). Scans were collected between 5 and 70° (2θ) with a step size of 0.02° and a scan rate of 5s

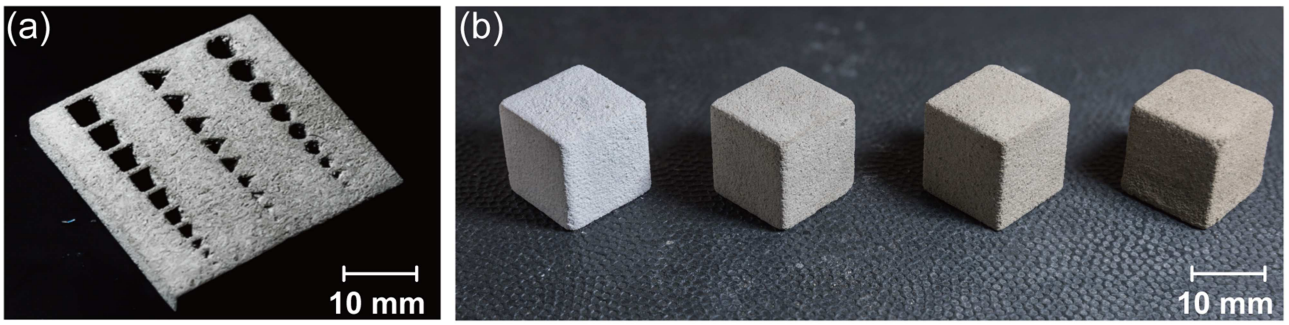

FIGURE 1 | 3D printed samples using the authors' developed geopolymer-based powder. **(a)** 40.4 × 40.4 × 5 mm plate structure with different holes. **(b)** 20 × 20 × 20 mm cubic samples. [Reprinted from Xia and Sanjayan (2016); Xia et al. (2018b) with permissions].

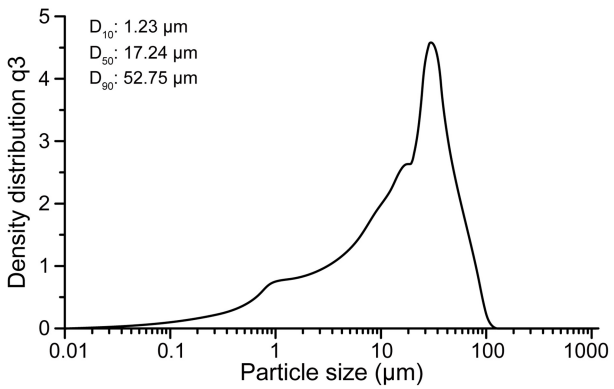

FIGURE 2 | Particle size distributions of the authors' developed 3D printable geopolymer powder.

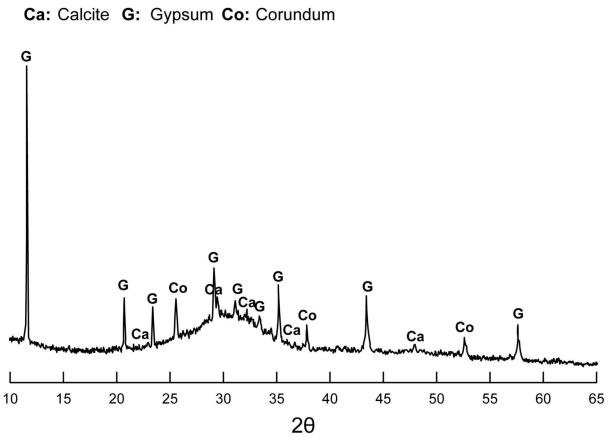

FIGURE 3 | X-ray diffraction analysis of slag. (Note: The corundum was added as internal standard for quantitative analysis).

per step. An internal standard (10 wt % corundum, Al_2O_3) was added to the raw slag to allow quantitative analysis using Rietveld refinement. As can be seen in **Figure 3**, a significant hump is shown between 25 and 35°. Calcite and gypsum crystalline phases are observed. The mineralogical phase percentages determined by using the Rietveld method are calcite (6.22%), gypsum (7.42%), and amorphous phase (86.36%).

Anhydrous sodium metasilicate powder (in the form of bead) supplied by Redox, Australia with the chemical composition of 50.66 wt Na_2O, 47.00 wt SiO_2 and 2.34 wt% H_2O was used as the alkaline activator. The alkaline activator beads were firstly ground for 5 min using a ball mill (Matest Jar Mill A091-10, MATEST system, Italy). The ceramic milling pot has a capacity of 300 cc and the ceramic ball has a diameter of 25 mm. For each batch, 150 grams of anhydrous sodium silicate beads were milled for 5 min at 400 RPM with powder/ball mass ratio of 0.3. A high purity silica sand with a median size of 184 µm supplied by TGS Industrial Sand Ltd., Australia was also used in this study.

Curing Mediums

Sodium hydroxide (NaOH) solution and potassium hydroxide (KOH) solution with 8.0 M concentration were prepared by dissolving NaOH and KOH flakes, respectively in tap water. The aim of using tap water, instead of distilled water, was to simulate the "real" condition at large-scale applications of the 3D printed geoplymers, in which condition it may not be easy and cost-effective to use distilled water. The NaOH and KOH flakes with a purity of 97% were both supplied by Sigma Aldrich Pty Ltd., Australia.

Two types of sodium silicate (Na_2SiO_3) solutions and two types of potassium silicate (K_2SiO_3) solutions were used in this study. All silicate solutions were supplied by PQ Australia Pty Ltd. The specifications of the silicate solutions are presented in **Table 1**.

Four different curing mediums, including two sodium (Na)-based alkaline solutions and two potassium (K)-based alkaline solutions were prepared as follows:

1. Na-based solution I (denoted as "Na-I"): composed of Na_2SiO_3- Grade D solution (71.4% w/w) and NaOH solution (28.6% w/w).
2. Na-based solution II (denoted as "Na-II"): composed of Na_2SiO_3-Grade N solution (71.4% w/w) and NaOH solution (28.6% w/w).

TABLE 1 | Specifications of the silicate solutions.

Silicate solutions	SiO_2^a (wt.%)	$M_2O^{a,b}$ (wt.%)	H_2O^a (wt.%)	Modulus^a (SiO_2/ M_2O^b)	Viscosity at 20°C (cps)^a
Na_2SiO_3-Grade D	29.4	14.7	55.9	2.00	250-450
Na_2SiO_3-Grade N	28.7	8.9	62.4	3.22	100-300
K_2SiO_3-Grade KASIL 1552	32.0	21.2	60.0	1.51	300-600
K_2SiO_3-Grade KASIL 2236	24.5	11.0	64.5	2.22	80-120

[a] *Average wt.% reported by the supplier.*
[b] *M in M_2O refers to Na or K.*

3. K-based solution I (denoted as "K-I"): composed of K_2SiO_3-Grade KASIL 1552 solution (71.4% w/w) and NaOH solution (28.6% w/w).
4. K-based solution II (denoted as "K-II"): composed of K_2SiO_3-Grade KASIL 2236 (71.4% w/w) and NaOH solution (28.6% w/w).

The alkali content (in terms of Na_2O or K_2O) and modulus of the four curing mediums used in this study are listed in **Table 2**. It should be noted that the selection of the type of NaOH and KOH solutions and Na_2SiO_3 and K_2SiO_3 solutions and the specific formulations of the curing mediums used in this study were based on the numerous research studies (e.g., Hardjito et al., 2004; Wallah and Rangan, 2006; Kong and Sanjayan, 2010; Nematollahi et al., 2014, 2017a,b) conducted by the authors and other researchers around the world on the production of geopolymer paste, mortar and concrete for "civil engineering" applications.

According to the alkali content and modulus listed in **Table 2** and the viscosity charts provided in Provis (2009) and PQ Corporation (2004), it can be inferred that the Na-I solution has higher viscosity than the Na-II solution at 20°C. Same trend is also true for the K-I and K-II solutions. According to Yang et al. (2008), the viscosity of sodium silicate solution decreases significantly with increasing temperature. The potassium silicate solutions also follow a similar trend (PQ Corporation, 2004). Therefore, based on the previous published data, it is assumed that the Na-II and K-II solutions have lower viscosity than that of the Na-I and K-I solutions. This is true regardless of the temperature.

3D Printing of Geopolymer Specimens

In this study, 20 mm cubic geopolymer specimens were printed using Zprinter® 150. The Zprinter® 150 is a commercial powder-based 3D printer manufactured by Z-Corp, USA with a specific resolution of 300 × 450 dpi, a build volume of 182 × 236 × 132 mm, and a build speed of 2–4 layers/min. It should be pointed out that at a resolution of 300 × 450 dpi, the minimum point size is 0.06 mm, which is much bigger than the median size of the printable powder (which is 17.24 μm as shown in **Figure 2**). The limiting factor on the resolution comes from the printer.

During the printing process, the binder liquid is jetted by HP11 print head, which requires a surface tension of approximately 45 dyn/cm and a viscosity of approximately 1.35 cP to function properly. An aqueous solvent (Zb® 63, Z-Corp, USA) was used as the binder during the printing process. The Zb® 63 binder was an aqueous commercial clear solution, composed of mainly water with 2-Pyrrolidone (Asadi-Eydivand et al., 2016), with the viscosity similar to pure water which does not react with the geopolymer powder.

TABLE 2 | The alkali content and modulus of the four curing mediums.

Curing mediums	M_2O^a (wt.%)	Modulus ($nSiO_2$/ nM_2O^a)
Na-I	17.4	1.47
Na-II	12.7	1.62
K-I	23.3	1.50
K-II	16.0	1.67

[a] *M in M_2O refers to Na or K.*

Figure 4 schematically illustrates the powder-based 3DCP process. First, a thin layer of powder is spread over the powder bed surface. Subsequently, binder droplets are selectively applied on the powder layer by a print-head, causing powder particles to bind to each other. The built part is completed by repeating the described steps and then is removed after certain drying time.

After the printing process completed, the samples were left undisturbed within the powder bed of the printer at room temperature for 6 h and then unbound powder was removed by using compressed air.

Post-processing and Testing Methods

After the de-powdering process, the printed cubes were divided into two groups denoted as "heat curing" and "ambient temperature curing".

For the "heat curing" group, the printed samples were immersed in each of the four curing mediums inside separate containers. The containers were sealed and placed in an oven at 60 ± 3°C for 7 days. After completion of the heat curing period, the containers were removed from the oven, and the heat cured samples were taken out from the curing mediums and kept undisturbed at ambient temperature (23 ± 3°C) and RH of 65% until the day of testing.

For the "ambient temperature curing" group, the printed samples were similarly immersed in each of the four curing mediums inside separate containers, but the sealed containers were kept at ambient temperature (23 ± 3°C) for 7 and 28 days. At the end of the curing period, the ambient temperature cured samples were taken out from the curing mediums and kept undisturbed until the day of testing. It should be pointed out

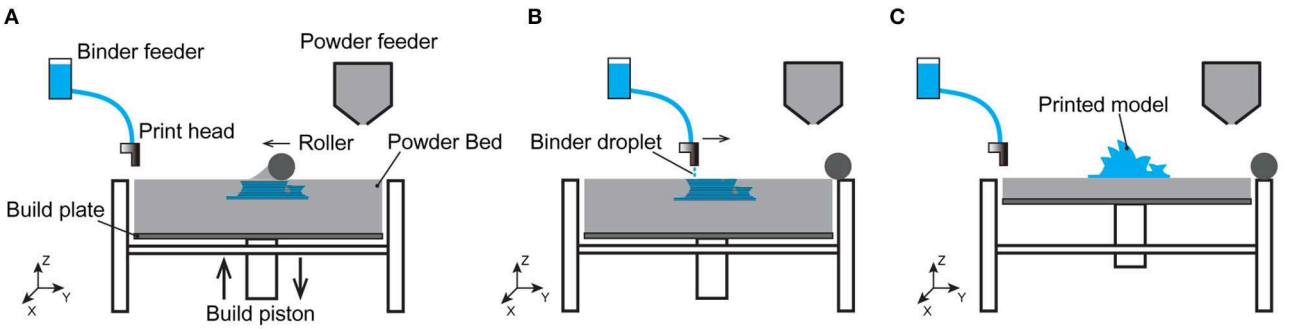

FIGURE 4 | Schematic illustration of the powder-based 3DCP process. **(A)** Powder spreading, **(B)** binder droplet deposition, **(C)** finished "green" sample.

that according to the authors' previous studies (Xia and Sanjayan, 2016, 2018), no dissolution of the "green" samples happened after being immersed in the curing mediums and subjected to heat/ambient temperature curing.

The heat cured specimens were tested at 7 days, while the ambient temperature cured samples were tested at 7 and 28 days. A population of 10 samples for each curing medium was used.

The apparent porosity of the printed cubic structures was measured based on Australian Standard AS 1774.5:2014. First of all, the samples were weighed in a dry state (M_{dry}) using a precision balance with an accuracy of 0.001 g, and then submerged in an immersion liquid for 30 min. Then, the weight of the samples suspended in the immersion liquid (M_{susp}) was measured. Subsequently, each sample was taken out from the immersion liquid and dabbed with a wet cloth to remove the excess immersion liquid and then was weighed to determine the wet weight (M_{wet}). The immersion liquid used in this study was ethanol (Reagent grade with 98% purity supplied by Sigma Aldrich Pty Ltd., Australia). The apparent porosity (P_{cube}) was calculated based on the following equations. A population of 10 samples for each curing medium was used.

$$\rho_{bulk.cube} = \rho_{liquid} \times \frac{M_{dry}}{M_{wet} - M_{susp}} \quad (1)$$

$$\rho_{cube} = 1 - \frac{\rho_{bulk.cube}}{\rho_{true.powder}} \times 100\% \quad (2)$$

The compressive strengths in both X-direction (i.e., the binder jetting direction) and Z-direction (i.e., layer stacking direction) were measured by an automated compressive strength testing machine (Technotest, Italy) under load control at the rate of 0.33 MPa/s. A population of 10 samples for each testing direction and curing medium was used.

RESULTS AND DISCUSSIONS

Heat Curing Group

Figure 5 shows the 7-day compressive strength of the heat cured 3D printed samples in two loading directions. In both directions, the compressive strength of the heat cured samples was significantly higher than that of the "green" strength. This

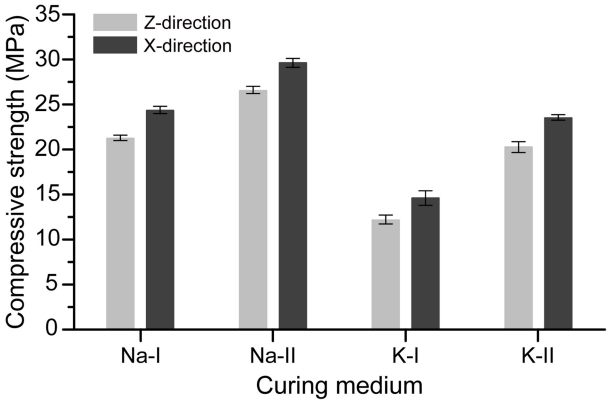

FIGURE 5 | Seven-day compressive strength of the heat cured 3D printed geopolymers. Note: The test result for the Na-II curing medium in the X-direction adopted from Xia and Sanjayan (2018). The error bars are calculated by standard deviation.

is true regardless of the type of curing medium. According to the authors' previous study (Xia and Sanjayan, 2016), the "green" strength of the printed sample is 0.76 ± 0.10 MPa in Z-direction and 0.91 ± 0.03 MPa in X-direction. The possible reason for the significantly higher compressive strength of the heat cured samples can be explained as follows:

Before the post-processing treatment, it is hypothesized that the "green" strength may come from the formation of calcium silicate hydrate due to the reaction among slag, sodium metasilicate powder and the liquid binder. However, during the post-processing treatment, when the green samples are immersed in the alkaline solutions, it is hypothesized that polymerization occurred within the sodium/potassium silicate solution, resulted in formation and development of geopolymeric products, which in turn led to the densification of porous structures of the "green" samples. As can be seen in **Table 3**, the apparent porosity of the heat-cured samples is far less than that of the "green" samples, which confirms the densification of the porous structure of the "green" samples. The exact reaction mechanism of these systems should be investigated in the future.

As can be seen in **Figure 5**, in both directions the 7-day compressive strength of the heat cured specimens immersed in the K-based solutions was lower than that of the specimens immersed in the Na-based solutions. This is attributed to the larger size of K^+ ion than Na^+ ion. According to Fernández-Jiménez et al. (2006), K^+ ion induces a lower crystallization speed of zeolites and slower development of pre-zeolitic gel due to its larger ion size, leading to lower compressive strength gain of the specimens immersed in the K-based solutions than the samples immersed in the Na-based solutions. It is worth to note that the Na-based liquid activators are generally cheaper than the K-based alkaline solutions (Nematollahi et al., 2015a, 2017a). Thereby, it can be concluded that for curing of "green" printed geopolymer samples, use of the Na-based alkaline solutions is highly beneficial in terms of lower cost and higher compressive strength gain, as compared to the K-based activators.

Among the Na-based solutions, according to **Figure 5**, the compressive strength of the heat cured samples immersed in the Na-II solution was 21–28% higher than that of the samples immersed in the Na-I solution, depending on the loading direction. The possible reasons for this result can be explained as follows:

As mentioned in Section Curing mediums, based on the previously published data, it is assumed that the viscosity of the Na-I solution is lower than that of the Na-II solution; thereby it is hypothesized that it can be relatively easier for the Na-II solution to penetrate into the "green" sample during the curing process, which favors the rate of geopolymerization reaction and compressive strength gain. The exact mechanism should be investigated in the future. In addition, the higher compressive strength of the heat cured samples immersed in the Na-II solution can also be due to the higher modulus of the Na-II solution than that of the Na-I solution (**Table 2**), which provides a higher amount of soluble silica in the Na-II solution. According to Xu and Van Deventer (2000), it is hypothesized that the higher amount of soluble silica in the Na-II solution accelerates the rate of geopolymerization reaction, thereby improves the compressive strength. Alshaaer (2013) has reported a similar curing method for kaolinite-based geopolymers by immersing them in an alkaline solution. The results of his study showed that secondary treatment (immersion in 6M NaOH solution at 80°C) led to an increase in the compressive strength and water resistance and a decrease in shrinkage of the samples.

For the heat-cured samples immersed in the K-based solutions, a similar trend was observed. The compressive strength of the heat cured samples immersed in K-II solution was about 61–66% higher than that of the specimens immersed in K-I solution, depending on the loading direction. Similar to the above discussion, this is due to the significantly lower viscosity and higher modulus of K-II solution than that of K-I solution.

As shown in **Figure 5**, an anisotropic phenomenon was observed in the compressive strength of the heat cured geopolymers depending on the loading directions. The compressive strength was always higher in the X-direction than in the Z-direction, regardless of the type of the curing medium. The ratios of the compressive strength in the X-direction to that in Z-direction (f_{c-x}/f_{c-z}) were listed in **Table 4**. The f_{c-x}/f_{c-z} of the samples immersed in the Na-II solution was higher than that of the Na-I solution. Similarly, the f_{c-x}/f_{c-z} of the samples immersed in the K-II solution was higher than that of the K-I solution. The higher f_{c-x}/f_{c-z} of the samples cured in the Na-II and K-II solutions might be related to the enhanced interlayer bond. According to Lowke et al. (2018), in powder-based 3D printed samples the water content significantly oscillates in accordance with a higher water content in the top region of the layer and a significantly lower content in the bottom region. In other words, the interlayer regions are more porous than other regions. Therefore, due to relatively lower viscosity of the Na-II and K-II solutions than the Na-I and K-I solutions (see Section Curing mediums), it is hypothesized that it is relatively easier for the Na-II and K-II solutions to transport to the pores in the interlayer regions and enhance the interlayer bond.

TABLE 3 | The apparent porosities of the green and 7-day heat-cured samples.

Samples	"Green"	Curing mediums			
		Na-I	Na-II	K-I	K-II
Apparent porosity (%)	57.4 ± 0.8	15.3 ± 0.7	13.6 ± 0.5	18.5 ± 1.1	15.6 ± 0.9

Each value is presented as mean ± standard deviation.

TABLE 4 | Anisotropy in the compressive strength of the heat cured 3D printed geopolymers.

Curing mediums	Na-I	Na-II	K-I	K-II
f_{c-x}/f_{c-z}	1.06	1.12	1.17	1.24

Ambient Temperature Curing Group

Figure 6 shows the 7-day and 28-day compressive strengths of the ambient temperature cured 3D printed samples in two loading directions. The 28-day compressive strength of the ambient temperature cured printed samples was higher than the 7-day compressive strength. This is true regardless of the testing direction and type of curing medium. This significant increase can be attributed to the continued geopolymerization process in the presence of alkaline solution, resulting in lower porosity of the samples cured for 28 days as compared to those cured for 7 days, as can be seen from **Table 5**. A similar result was reported for the conventionally mold-casting geopolymers, where the longer curing time increased the compressive strength (Nematollahi et al., 2015b; Wongsa et al., 2018).

According to **Figure 6**, the compressive strength of the ambient temperature cured printed specimens immersed in the K-based solutions was generally lower than that of the specimens immersed in the Na-based solutions. This is true regardless of the age of curing. As discussed in Section Heat curing group, a similar trend was also observed for the heat cured printed specimens (**Figure 5**). The reason for the lower strength of the specimens immersed in the K-based solutions than that of the specimens

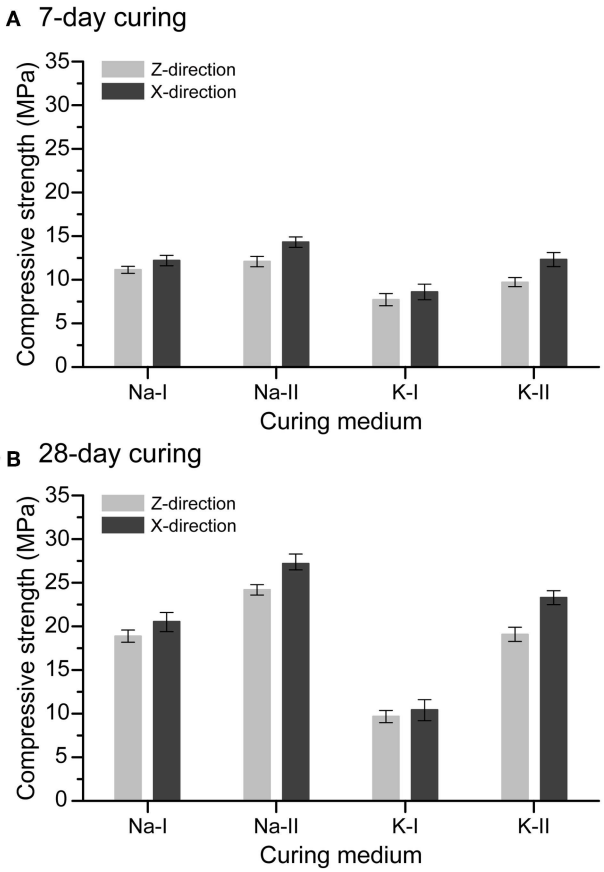

FIGURE 6 | Compressive strength of the ambient temperature cured 3D printed geopolymers at **(A)** 7 days and **(B)** 28 days. The error bars are calculated by standard deviation.

TABLE 5 | The apparent porosities of the 7- and 28-day ambient temperature cured samples.

Curing mediums	Apparent porosities (%)	
	7-day	28-day
Na-I	21.2 ± 0.9	15.5 ± 1.3
Na-II	19.5 ± 1.3	13.2 ± 0.9
K-I	27.6 ±1.4	22.5 ± 1.5
K-II	23.6 ± 0.6	20.2 ± 0.7

Each value is presented as mean ± standard deviation.

immersed in the Na-based solutions is explained in Section Heat curing group.

As can be seen in **Figure 6**, the compressive strength of the ambient temperature cured printed samples immersed in the Na-II solution was higher than that of the specimens immersed in the Na-I solution. In addition, the compressive strength of the ambient temperature cured printed samples immersed in the K-II solution was higher than that of the specimens immersed in the K-I solution. These are true regardless of testing direction and age of curing. As discussed in Section Heat curing group, a similar trend was also observed for the heat cured printed specimens (**Figure 5**). The reason for the higher strength of the specimens immersed in the Na-II or K-II solutions than that of the specimens immersed in the Na-I or K-I solutions is explained in Section Heat curing group.

TABLE 6 | Anisotropy in the compressive strength of the ambient temperature cured 3D printed geopolymers.

	Curing mediums			
	Na-I	Na-II	K-I	K-II
f_{c-x}/f_{c-z} at 7 days	1.09	1.18	1.11	1.27
f_{c-x}/f_{c-z} at 28 days	1.08	1.13	1.07	1.22

Similar to the heat cured specimens (**Figure 5**), the compressive strength of the ambient temperature cured printed specimens also exhibited similar anisotropic behavior, depending on the loading direction. The compressive strength was always higher in the X-direction than in the Z-direction, regardless of the type of curing medium and age of curing. The f_{c-x}/f_{c-z} ratios were listed in **Table 6**. The f_{c-x}/f_{c-z} of the Na-II solution cured samples was higher than that of the Na-I solution cured samples. In addition, the f_{c-x}/f_{c-z} of the K-II solution cured samples was higher than that of the K-I solution cured samples. These trends are true regardless of the age of curing. As discussed in Section Heat curing group, a similar trend was also observed for the heat cured printed specimens (**Figure 5**). The reason for the higher f_{c-x}/f_{c-z} of the samples cured in the Na-II and K-II solutions is explained in Section Heat curing group. It is worth noting that the increase in age of curing (from 7 days to 28 days) slightly reduced the observed anisotropic behavior in the compressive strength results.

Among the curing mediums investigated, according to **Figures 5**, **6**, the printed samples immersed in the K-I solution exhibited the lowest compressive strength. This is true regardless of the type and age of curing, as well as the testing direction. This is because of the very high viscosity and the low modulus of the K_2SiO_3-Grade KASIL 1552 solution used to prepare the K-I solution, which makes this solution not as effective as the other curing mediums.

Comparison between **Figures 5**, **6B** showed that, except for the samples immersed in the K-I solution, the 28-day compressive strength of the ambient temperature cured printed samples was only up to 8% lower than the 7-day compressive strength of the corresponding heat cured printed samples. Therefore, the feasibility of the developed post-processing method based on the ambient temperature curing for enhancing the strength of powder-based 3D printed geopolymers is established, which requires less energy, yet provides comparable strength as compared to the previously developed post-processing method based on the heat curing. At the same time, eliminating the necessity for the heat curing reduces the complexity (and therefore likely cost) of the production process, and therefore enhances the commercial viability of the developed powder-based 3D printed geopolymers in the construction industry.

CONCLUSIONS

This study focused on the post-processing (i.e., curing) techniques to improve the compressive strength of the geopolymers made by the powder-based 3D printing process for construction applications. The effects of type of curing medium, curing temperature, duration of curing, and loading direction on the compressive strength of the powder-based 3D printed geopolymers were experimentally evaluated. The following conclusions are drawn:

1) The compressive strength of the printed geopolymer sample cured at ambient temperature (23°C) for 28 days was comparable to that of the sample cured at elevated temperature (60°C) for 7 days. This is true regardless of the type of curing medium, and testing direction. Achieving the comparable strength without the necessity for heat curing reduces the complexity (and therefore likely cost) of the production process, and therefore enhances the commercial viability of the developed powder-based 3D printed geopolymers in the construction industry.
2) For post-processing of the "green" samples under the heat curing condition, the Na-based activators were highly beneficial in terms of higher compressive strength gain and lower cost as compared to the K-based activators. This is true regardless of the testing direction and modulus of the activator solution.
3) Among the Na-based curing mediums, the Na-II activator containing the Na_2SiO_3 solution with a higher alkali modulus of 3.22 and a lower viscosity (N Grade) was the most effective in increasing the compressive strength of the printed geopolymers, as compared to the Na-I activator containing the Na2SiO3 solution with a lower alkali modulus of 2.00 and a higher viscosity (D Grade). This is true regardless of the duration and temperature of curing, and testing direction.
4) Among the K-based curing mediums, the K-II activator containing the K_2SiO_3 solution with a higher alkali modulus of 2.22 and a lower viscosity (KASIL 2236 Grade) was the most effective in increasing the compressive strength of the printed geopolymers, as compared to the K-I activator containing the K_2SiO_3 solution with a lower alkali modulus of 1.51 and a higher viscosity (KASIL 1552 Grade). This is true irrespective of the duration and temperature of curing, and testing direction.
5) The compressive strength of the printed geopolymers exhibited an anisotropic behavior, depending on the testing direction. The compressive strength was always higher in the binder jetting direction (X-direction) than in the layer stacking direction (Z-direction). This is true irrespective of the type of the curing medium, and duration and temperature of curing.
6) The 28-day compressive strength of the ambient temperature cured printed geopolymer samples was considerably higher than the 7-day compressive strength. This is true regardless of the testing direction and type of curing medium. This result is consistent with that reported in the literature for conventionally mold-cast geopolymer where the longer curing period results in higher compressive strength.

AUTHOR CONTRIBUTIONS

BN and JS jointly secured the grants and designed the research project. BN designed the experimental plan of this paper. MX performed the experimental work. MX and BN jointly interpreted the results and wrote the draft of the paper. JS reviewed and edited the paper.

ACKNOWLEDGMENTS

Authors acknowledge the support by the Australian Research Council Discovery Grant DP170103521 and Linkage Infrastructure Grant LE170100168 and Discovery Early Career Researcher Award DE180101587.

REFERENCES

Al-Sanabani, J. S., Madfa, A. A., and Al-Sanabani, F. A. (2013). Application of calcium phosphate materials in dentistry. *Int. J. Biomater.* 2013:876132. doi: 10.1155/2013/876132

Alshaaer, M. (2013). Two-phase geopolymerization of kaolinite-based geopolymers. *Appl. Clay Sci.* 86, 162–168. doi: 10.1016/j.clay.2013.10.004

Asadi-Eydivand, M., Solati-Hashjin, M., Shafiei, S. S., Mohammadi, S., Hafezi, M., and Osman, N. A. A. (2016). Structure, properties, and *In Vitro* behavior of heat-treated calcium sulfate scaffolds fabricated by 3D printing. *PloS ONE* 11:e0151216. doi: 10.1371/journal.pone.0151216

Bai, Y., and Williams, C. B. (2015). An exploration of binder jetting of copper. *Rapid Prototyping J.* 21, 177–185. doi: 10.1108/RPJ-12-2014-0180

Biernacki, J. J., Bullard, J. W., Sant, G., Brown, K., Glasser, F. P., Jones, S., et al. (2017). Cements in the 21st century: challenges, perspectives, and opportunities. *J. Am. Ceram. Soc.* 100, 2746–2773. doi: 10.1111/jace.14948

Cesaretti, G., Dini, E., De Kestelier, X., Colla, V., and Pambaguian, L. (2014). Building components for an outpost on the lunar soil by means of a novel 3D printing technology. *Acta Astronaut.* 93, 430–450. doi: 10.1016/j.actaastro.2013.07.034

De Schutter, G., Lesage, K., Mechtcherine, V., Nerella, V. N., Habert, G., and Agusti-Juan, I. (2018). Vision of 3D printing with concrete—technical, economic and environmental potentials. *Cement Concrete Res.* 112, 25–36. doi: 10.1016/j.cemconres.2018.06.001

Duxson, P., Fernández-Jiménez, A., Provis, J. L., Lukey, G. C., Palomo, A., and Deventer, J. S. J. (2006). Geopolymer technology: the current state of the art. *J. Mater. Sci.* 42, 2917–2933. doi: 10.1007/s10853-006-0637-z

Duxson, P., Provis, J. L., Lukey, G. C., and Van Deventer, J. S. (2007). The role of inorganic polymer technology in the development of 'green concrete'. *Cement Concrete Res.* 37, 1590–1597. doi: 10.1016/j.cemconres.2007.08.018

ExOne (2015). *Exerial Industrial Production 3D Printer*. Available online at: https://www.exone.com/Systems/Production-Printers/-Exerial (accessed June 12, 2019).

Fernández-Jiménez, A., Palomo, A., and Criado, M. (2006). Alkali activated fly ash binders. a comparative study between sodium and potassium activators. *Mater Construcción* 56, 51–65. doi: 10.3989/mc.2006.v56.i281.92

Gaytan, S., Cadena, M., Karim, H., Delfin, D., Lin, Y., Espalin, D., et al. (2015). Fabrication of barium titanate by binder jetting additive manufacturing technology. *Ceram. Int.* 41, 6610–6619. doi: 10.1016/j.ceramint.2015.01.108

Gibbons, G. J., Williams, R., Purnell, P., and Farahi, E. (2010). 3D Printing of cement composites. *Adv. Appl. Ceram.* 109, 287–290. doi: 10.1179/174367509X12472364600878

Hardjito, D., Wallah, S. E., Sumajouw, D. M. J., and Rangana, B. V. (2004). On the development of fly ash-based geopolymer concrete. *Aci. Mater. J.* 101, 467–472. doi: 10.14359/13485

Huntzinger, D. N., and Eatmon, T. D. (2009). A life-cycle assessment of portland cement manufacturing: comparing the traditional process with alternative technologies. *J. Clean Prod.* 17, 668–675. doi: 10.1016/j.jclepro.2008.04.007

Khoshnevis, B. (2004). Automated construction by contour crafting—related robotics and information technologies. *Automat. Constr.* 13, 5–19. doi: 10.1016/j.autcon.2003.08.012

Kong, D. L., and Sanjayan, J. G. (2010). Effect of elevated temperatures on geopolymer paste, mortar and concrete. *Cement Concrete Res.* 40, 334–339. doi: 10.1016/j.cemconres.2009.10.017

Le, T. T., Austin, S. A., Lim, S., Buswell, R. A., Gibb, A. G. F., and Thorpe, T. (2012a). Mix design and fresh properties for high-performance printing concrete. *Mater. Struct.* 45, 1221–1232. doi: 10.1617/s11527-012-9828-z

Le, T. T., Austin, S. A., Lim, S., Buswell, R. A., Law, R., Gibb, A. G. F., et al. (2012b). Hardened properties of high-performance printing concrete. *Cement Concrete Res.* 42, 558–566. doi: 10.1016/j.cemconres.2011.12.003

Li, Z., Ding, Z., and Zhang, Y. (2004). "Development of sustainable cementitious materials," in: *Proceedings of International Workshop on Sustainable Development and Concrete Technology*. (Beijing). Available online at: http://publications.iowa.gov/2941/1/SustainableConcreteWorkshop.pdf#page=66 (accessed June 5, 2019).

Lloret, E., Shahab, A. R., Linus, M., Flatt, R. J., Gramazio, F., Kohler, M., et al. (2015). Complex concrete structures: merging existing casting techniques with digital fabrication. *Comput. Aided Desig.* 60, 40–49. doi: 10.1016/j.cad.2014.02.011

Lowke, D., Dini, E., Perrot, A., Weger, D., Gehlen, C., and Dillenburger, B. (2018). Particle-bed 3D printing in concrete construction–possibilities and challenges. *Cement Concrete Res.* 112, 50–65. doi: 10.1016/j.cemconres.2018.05.018

Maier, A. K., Dezmirean, L., Will, J., and Greil, P. (2011). Three-dimensional printing of flash-setting calcium aluminate cement. *J. Mater. Sci.* 46, 2947–2954. doi: 10.1007/s10853-010-5170-4

Marchon, D., Kawashima, S., Bessaies-Bey, H., Mantellato, S., and Ng, S. (2018). Hydration and rheology control of concrete for digital fabrication: potential admixtures and cement chemistry. *Cement Concrete Res.* 112, 96–110. doi: 10.1016/j.cemconres.2018.05.014

Mccaffrey, R. (2002). Climate change and the cement industry. *Glob. Cem. Lime. Mag.* 15–19.

Moon, J., Caballero, A. C., Hozer, L., Chiang, Y.-M., and Cima, M. J. (2001). Fabrication of functionally graded reaction infiltrated SiC–Si composite by three-dimensional printing (3DP^{TM}) process. *Mater. Sci. Eng. A.* 298, 110–119. doi: 10.1016/S0921-5093(00)01282-X

Nandwana, P., Elliott, A. M., Siddel, D., Merriman, A., Peter, W. H., and Babu, S. S. (2017). Powder bed binder jet 3D printing of Inconel 718: Densification, microstructural evolution and challenges. *Curr. Opin. Solid St. M.* 21, 207–218. doi: 10.1016/j.cossms.2016.12.002

Nematollahi, B., Qiu, J., Yang, E.-H., and Sanjayan, J. (2017a). Micromechanics constitutive modelling and optimization of strain hardening geopolymer composite. *Ceram Int.* 43, 5999–6007. doi: 10.1016/j.ceramint.2017.01.138

Nematollahi, B., Qiu, J., Yang, E.-H., and Sanjayan, J. (2017b). Microscale investigation of fiber-matrix interface properties of strain-hardening geopolymer composite. *Ceram Int.* 43, 15616–15625. doi: 10.1016/j.ceramint.2017.08.118

Nematollahi, B., Sanjayan, J., and Ahmed Shaikh, F. U. (2015a). Tensile strain hardening behavior of PVA fiber-reinforced engineered geopolymer composite. *J. Mater. Civil. Eng.* 27:04015001. doi: 10.1061/(ASCE)MT.1943-5533.0001242

Nematollahi, B., Sanjayan, J., and Shaikh, F. U. A. (2014). Comparative deflection hardening behavior of short fiber reinforced geopolymer composites. *Constr. Build. Mater.* 70, 54–64. doi: 10.1016/j.conbuildmat.2014.07.085

Nematollahi, B., Sanjayan, J., and Shaikh, F. U. A. (2015b). Synthesis of heat and ambient cured one-part geopolymer mixes with different grades of sodium silicate. *Ceram Int.* 41, 5696–5704. doi: 10.1016/j.ceramint.2014.12.154

Nematollahi, B., Xia, M., and Sanjayan, J. (2017c). "Current progress of 3D concrete printing technologies," in: *ISARC Proceedings of the International Symposium on Automation and Robotics in Construction*. (Taipei: Vilnius Gediminas Technical University, Department of Construction Economics & Property).

PQ Corporation (2004). *Sodium and Potassium Silicates*. Available online at: https://www.pqcorp.com/docs/default-source/recommended-literature/pq-corporation/lithium-silicate/sodium-and-potassium-silicates-brochure-eng-oct-2004.pdf?sfvrsn=d22426fb_3 (accessed June 5, 2019).

Provis, J. L. (2009). "Activating solution chemistry for geopolymers," in *Geopolymers Structures, Processing, Properties and Industrial Applications*. Series in Civil and Structural Engineering, eds J. L. Provis and J. S. J. van Deventer (Woodhead Publishing), 50–71. doi: 10.1533/9781845696382.frontmatter

Rael, R., and San Fratello, V. (2011). "Developing concrete polymer building components for 3D printing," in: *ACADIA. 31st Annual Conference of the Association for Computer Aided Design in Architecture*. (Banff). Available online at: http://www.rael-sanfratello.com/media/emerging_objects/papers/243.pdf (accessed June 5, 2019).

Roussel, N. (2018). Rheological requirements for printable concretes. *Cement Concrete Res.* 112, 76–85. doi: 10.1016/j.cemconres.2018.04.005

Sanjayan, J. G., and Nematollahi, B. (2019). "3D concrete printing for construction applications," in *3D Concrete Printing Technology*. Melbourne, VIC: Elsevier, 1–11.

Shanjani, Y., and Toyserkani, E. (2008). "Material spreading and compaction in powder-based solid freeform fabrication methods: Mathematical modeling," in: *19th Annual International Solid Freeform Fabrication Symposium, SFF 2008*), 399–410. Available online at: http://edge.rit.edu/edge/P10551/public/SFF/SFF%202008%20Proceedings/Manuscripts/2008-36-Shanjani.pdf (accessed June 5, 2019).

Voxeljet (2016). *Largest Industrial 3D Sand Printing System in the World: The VX4000*. Available online at: https://www.voxeljet.com/3d-printing-systems/vx4000/ (accessed 12, June 2019).

Wallah, S., and Rangan, B. V. (2006). *Low-Calcium Fly Ash-Based Geopolymer Concrete: Long-Term Properties*. Available online at: https://www.geopolymer.org/fichiers_pdf/curtin_flyash_GC-2.pdf (accessed June 5, 2019).

Wangler, T., Lloret, E., Reiter, L., Hack, N., Gramazio, F., Kohler, M., et al. (2016). Digital concrete: opportunities and challenges. *RILEM Tech. Lett.* 1, 67–75. doi: 10.21809/rilemtechlett.2016.16

Wongsa, A., Sata, V., Nematollahi, B., Sanjayan, J., and Chindaprasirt, P. (2018). Mechanical and thermal properties of lightweight geopolymer mortar incorporating crumb rubber. *J. Clean Prod.* 195, 1069–1080. doi: 10.1016/j.jclepro.2018.06.003

Wu, P., Wang, J., and Wang, X. (2016). A critical review of the use of 3-D printing in the construction industry. *Automat. Constr.* 68, 21–31. doi: 10.1016/j.autcon.2016.04.005

Xia, M., Nematollahi, B., and Sanjayan, J. (2018a). Influence of binder saturation level on compressive strength and dimensional accuracy of powder-based 3D printed geopolymer. *Mater. Sci. Forum.* 939, 177–183. doi: 10.4028/www.scientific.net/MSF.939.177

Xia, M., Nematollahi, B., and Sanjayan, J. (2018b). Printability, accuracy and strength of geopolymer made using powder-based 3D printing for construction applications. *Automat. Constr.* 101, 179–189. doi: 10.1016/j.autcon.2019.01.013

Xia, M., and Sanjayan, J. (2016). Method of formulating geopolymer for 3D printing for construction applications. *Mater. Design* 110, 382–390. doi: 10.1016/j.matdes.2016.07.136

Xia, M., and Sanjayan, J. (2018). Methods of enhancing strength of geopolymer produced from powder-based 3D printing process. *Mater. Lett.* 227, 281–283. doi: 10.1016/j.matlet.2018.05.100

Xu, H., and Van Deventer, J. S. J. (2000). The geopolymerisation of alumino-silicate minerals. *Int. J. Miner. Process* 59, 247–266. doi: 10.1016/S0301-7516(99)00074-5

Yang, X., Zhu, W., and Yang, Q. (2008). The viscosity properties of sodium silicate solutions. *J. Solution Chem.* 37, 73–83. doi: 10.1007/s10953-007-9214-6

Zhou, Z., Buchanan, F., Mitchell, C., and Dunne, N. (2014). Printability of calcium phosphate: calcium sulfate powders for the application of tissue engineered bone scaffolds using the 3D printing technique. *Mater. Sci. Eng. C.* 38, 1–10. doi: 10.1016/j.msec.2014.01.027

Conflict of Interest Statement: The authors declare that the research was conducted in the absence of any commercial or financial relationships that could be construed as a potential conflict of interest.